Geophysical Research Letters

RESEARCH LETTER
10.1029/2019GL085522

Precise Detections of Solar Particle Events and a New View of the Moon

Jody K. Wilson[1,2], Harlan E. Spence[1,2], Nathan A. Schwadron[1,2], Anthony W. Case[3], Mark D. Looper[4], Andrew P. Jordan[1,2], Wouter de Wet[1], and Justin Kasper[5]

[1]Institute for the Study of Earth, Oceans, and Space, University of New Hampshire, Durham, NH, USA, [2]Solar System Exploration Research Virtual Institute, NASA Ames Research Center, Moffet Field, CA, USA, [3]Harvard-Smithsonian Center for Astrophysics, Cambridge, MA, USA, [4]The Aerospace Corporation, El Segundo, CA, USA, [5]Michigan Institute for Research in Astrophysics, University of Michigan, Ann Arbor, MI, USA

Key Points:
- The CRaTER instrument on LRO can detect and quantify small solar particle events with a simple new analysis technique
- Our new lunar map of albedo radiation resembles gamma ray maps from Lunar Prospector
- Follow-up studies will investigate contributions from neutrons, protons, and gamma rays, and signatures of hydrogen in lunar regolith

Supporting Information:
- Supporting Information S1
- Figure S1
- Figure S2
- Figure S3
- Figure S4

Correspondence to:
J. K. Wilson,
jody.wilson@unh.edu

Citation:
Wilson, J. K., Spence, H. E., Schwadron, N. A., Case, A. W., Looper, M. D., Jordan, A. P., et al. (2020). Precise detections of solar particle events and a new view of the moon. *Geophysical Research Letters*, *47*, e2019GL085522. https://doi.org/10.1029/2019GL085522

Received 23 SEP 2019
Accepted 18 DEC 2019
Accepted article online 23 DEC 2019

Additional author notes should be indicated with symbols (for example, for current addresses).

Abstract We have invented a new method for detecting solar particle events using data from the Cosmic Ray Telescope for the Effects of Radiation (CRaTER) on the Lunar Reconnaissance Orbiter (LRO). Using a simple function of the total particle detection rates from four of CRaTER's six detectors, we can precisely identify solar energetic particle event periods in the CRaTER data archive. During solar quiet periods we map the distribution of a mare-associated mixture of elements in the lunar regolith using this new method. The new map of the moon probably reflects an as-yet unknown combination of lunar albedo protons, neutrons, and gamma rays, and most closely resembles Lunar Prospector maps of gamma rays characteristic of thorium and iron. This result will lead to multiple follow-up studies of lunar albedo particles and may also contribute to the study of diurnally varying hydrogenation of the lunar regolith.

1. Introduction

The Cosmic Ray Telescope for the Effects of Radiation (CRaTER) instrument on Lunar Reconnaissance Orbiter (LRO; Spence et al., 2010) measures the lineal energy transfer of radiation in matter due to galactic cosmic rays (GCRs; e.g., Case et al., 2013) and solar energetic particles (SEPs). CRaTER is a cylindrical stack of six solid state detectors (D1 through D6), nominally oriented with detector D1 facing zenith and D6 facing the nadir point on the Moon's surface (Figure 1). The thin (148 μm) detectors (D1, D3, D5) are designed to measure heavy ions without saturating and are each paired with a more sensitive thick (1 mm) detector (D2, D4, D6). Two pieces of tissue equivalent plastic (TEP) separate the three pairs, so that detectors D1 and D2 are exposed to the zenith, D5 and D6 are exposed to the nadir direction, and D3 and D4, sandwiched between the two pieces of TEP, are moderately shielded from both nadir and zenith.

CRaTER has been measuring GCRs and SEPs from lunar orbit since June 2009. As CRaTER can detect particles arriving from any direction, it also detects various nuclear spallation products propagating up from the Moon (Looper et al., 2013; Spence et al., 2013); thanks to LRO's polar orbit (average altitude ~50–90 km), we can make maps of the flux of such "albedo" particles and search for surface features in elemental composition that might affect the albedo proton yield, in a manner similar to the Lunar Prospector gamma ray instrument (Lawrence et al., 1998; Prettyman et al., 2006) and neutron detectors on Lunar Prospector and LRO (e.g., Elphic et al., 2000; Mitrofanov et al., 2010; Litvak, Mitrofanov, Sanin, Malakhov, et al., 2012). Wilson et al. (2012) attempted the first mapping of lunar albedo protons using the first 18 months of CRaTER data to demonstrate the methodology. Subsequent work included more data coverage in the albedo proton map (Wilson et al., 2014), but the data reduction method was never able to discern features with sufficient statistical significance.

We were more successful in mapping lunar albedo proton yields by reducing spatial resolution and by improving the data reduction method. Schwadron et al. (2016) binned several years of CRaTER data by lunar latitude and found a latitudinal trend in the albedo proton yield, suggesting a detection of high-latitude (polar) hydrogen or H-bearing molecules. Also, an improved data analysis technique tentatively discerned a sunrise-versus-sunset contrast in the albedo proton yield using only a small fraction of the CRaTER data set (Schwadron et al., 2018), suggesting a diurnal variation in the hydrogenation of the lunar regolith.

The CRaTER instrument produces two parallel data streams; the extensively used primary science data records the amount of energy deposited in each of the six detectors whenever an ionizing particle passes

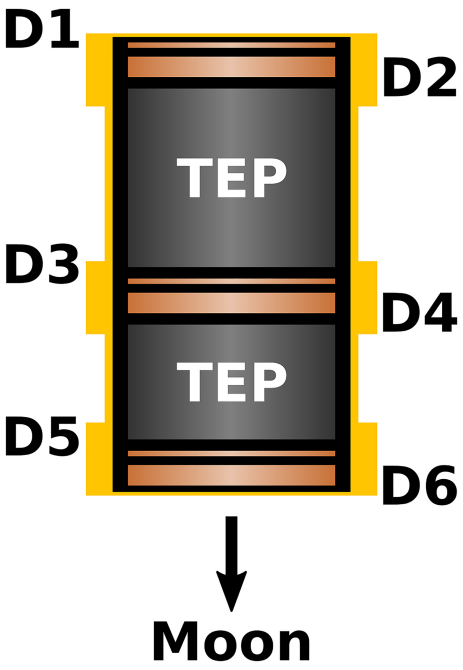

Figure 1. Illustrative diagram of the CRaTER instrument (detailed description in Spence et al., 2010) showing the arrangement of six detectors (D1 through D6) and two pieces of tissue-equivalent plastic (TEP). Each detector pair consists of one thin, odd-numbered detector and one thick, even-numbered detector. The detector pairs are ringed by extra shielding (yellow) to reduce the sensitivity to side-penetrating particles. The D1 detector faces deep space in the nominal spacecraft attitude, while the D6 detector faces the Moon. Detectors D3 and D4 are the most shielded, as they have TEP blocking both the zenith and nadir directions.

through at least one detector. The amount of energy deposited is represented as one of 4,096 energy channels, and the thin and thick detectors have different, but overlapping, energy ranges. CRaTER's primary data have been used for nearly every study to date, including solar cycle trends (e.g., Schwadron et al., 2014) shielding effects and dose rates (e.g., Zeitlin et al., 2013), solar particle events (e.g., Joyce et al., 2013), and the albedo proton mapping studies.

The secondary data stream, on the other hand, comprises a simpler accounting of ionizing particles that pass through each detector. Every such particle generates a "singles event," incrementing the singles counter for the detector (or detectors, if two or more were impinged upon) by one, regardless of the direction, type, or amount of energy deposited by the particle; the low-energy threshold for a singles event is lower than in primary data. Here we demonstrate an unanticipated application of secondary data that can discern small solar particle events and map the distribution of albedo particles coming from the Moon in a new way.

2. Identifying SEP Events in CRaTER Data

Galactic cosmic rays are responsible for most of the nuclear spallation products produced from the lunar regolith during nominal (solar quiet) conditions. They are ever-present, slowly varying, and bathe the Earth-Moon system approximately isotropically. The GCR spectrum peaks at an energy range of several hundred MeV per nucleon but varies over the course of the solar cycle (e.g., Potgieter, 2013). Most GCRs have enough energy to pass completely through the CRaTER instrument, and thus register in all three of CRaTER's thick detectors at approximately the same rates, and in all three thin detectors at lower rates. GCRs striking the Moon can initiate several types of nuclear spallation reactions and collisional cascades, resulting in the ejection of many particle types and photons from the lunar surface and back into space where CRaTER can detect them (Looper et al., 2013; Spence et al., 2013).

SEPs compose the majority of the remaining energetic particle population impinging on the lunar surface and on the CRaTER instrument. SEP events occur intermittently during solar active periods and exhibit a wide range of energies and fluxes (e.g.,Desai & Giacalone, 2016), but usually dominate the total particle detection rate on CRaTER when an event is underway. Compared to GCRs, SEPs usually have softer energy spectra and on average have a lower spallation yield in the lunar regolith. These large differences between SEPs and GCRs mean we cannot use our nominal data reduction methods during SEP events, and our solution for mapping studies is simply to exclude data taken during SEP events.

Planetary and heliophysics studies that use CRaTER data require proper identification of all SEP events in the data set to either cull SEP periods from GCR studies, as in the mapping studies, or to study the effects of SEP events themselves (e.g., Joyce et al., 2013). While there are data from other near-Earth spacecraft that could be used to identify events, CRaTER has the advantage of measuring the instantaneous particle environment at the Moon at the energies of interest.

We have tried different techniques for identifying SEP events in CRaTER data with varying degrees of success. Wilson et al. (2012, 2014) and Schwadron et al. (2016) used a trailing moving average of CRaTER singles rates as a proxy for the GCR background trend and compared it with a shorter-term average of the singles rate to judge whether an SEP event was underway at any given time. This method is flawed by the effects of any long-term increase or decrease in the GCR background, and by active periods which tend to increase the calculated moving average to a level well above the actual GCR background. (A similar method with a related limitation is used by the GOES team to identify SEP events in their data; they use a high event detection threshold due to the varying GCR background.) More recent work by Schwadron et al. (2018) used only ~500 hr of CRaTER data, so it could rely on the visual identification of three small SEP events to manually isolate periods where only the GCR background was present. This, however, is impractical for multiyear

analysis and might suffer from a lack of consistency. We thus seek a simple function that algorithmically converts CRaTER data into an index that will reliably distinguish SEP event times from periods with no SEPs.

3. SEP Index

We developed the SEP Index (SEPI), which is a function of the total singles detection rates from four of CRaTER's six detectors: D1, D3, D4, and D6:

$$\mathrm{SEPI} = 0.144*\mathrm{D1s}/\mathrm{D3s} + 0.446*\mathrm{D1s}/\mathrm{D4s} + 0.792*\mathrm{D6s}/\mathrm{D4s} \quad (1)$$

where DNs is the number of singles events recorded in detector N during a given period or over a given location on the Moon. (A description of the empirical derivation of the SEPI factors is given in the supporting information.) The index makes use of D1 (zenith) and D6 (nadir) being the outermost and least-shielded detectors; in other words, they are most exposed to SEPs, which have much lower average energies than GCRs. The index also uses the singles rates of detectors D3 and D4 as proxies for the flux of the more penetrating GCR background because they are the innermost detectors with the highest overall shielding.

As shown in the plot of the SEP Index versus time (Figure 2), even small SEP events stand out cleanly from the GCR background, which is remarkably flat over the 8.5-year period. Without regard for the physical mechanism(s) at work, we crafted this weighted sum of three singles rate ratios to minimize the temporal trends in the GCR background, starting from the principal of comparing “outer” exposed detectors to “inner” shielded detectors. We note that the SEP Index is constant to within ~1% during solar quiet times during the entire LRO mission. We next investigate the usefulness of the index's value during SEP events.

4. The CRaTER SEP Index Quantification of SEP Events

The magnitude of the SEP Index during SEP events is approximately correlated with peak proton flux measured concurrently by the GOES satellite network in geostationary orbit (Gurman, 2017). We define an SEP event as any ≥4-hr period where the hourly SEP Index is always >1.02; in practice this avoids misidentifying statistical noise fluctuations in the data. Figure 3 shows the relationship between the peak CRaTER SEP Index during each SEP event and GOES maximum proton fluxes in three energy channels. All events in the GOES SEP event list are recognized by the SEPI method, but the GOES SEP event list does not publish events with maximum fluxes less than 10 pfu; thus, the GOES maximum flux in Figure 3 was determined by taking the maximum of the 5-min averaged proton flux observed at either the GOES 14 or GOES 15 spacecraft over the time period for each SEPI event. We are not attempting to prove that there is any precise quantification here, only that there is some meaning to the magnitude of the SEP Index during SEP events. As designed and desired, the SEP Index identifies a large number of small events, the goal needed to robustly remove their effects from the data set before constructing maps.

5. Mapping the Moon With the SEP Index

During solar quiet times, the SEPI is affected by neither season, orbital altitude of LRO, nor any other known periodicity; thus, we next search for any sensitivity of SEPI to location over the Moon by mapping SEPI using all solar quiet times (no SEP events) from the start of the LRO mission through the end of 2017. When the hourly average of SEPI is at least 1.02 we do not include that hour of data in the map. When SEPI is below 1.02, and LRO/CRaTER is pointed at nadir and operating nominally, we add singles data to its corresponding locations in four $1° \times 1°$ maps of D1s, D3s, D4s, and D6s. Whereas we bin data in time (hourly) for culling SEP events with the SEP Index, we bin data spatially by 1° in latitude and longitude for mapping. Once all the data have been registered in the 1° maps, we bin the maps into larger pixels ($10° \times 10°$) and then apply the SEPI function (equation (1)) to each large pixel. Figure 4 shows the resulting map.

The lunar SEP Index map shown in Figure 4 shows an ~0.5% higher average signal in the lunar mare compared to the lunar highlands, and at first glance resembles some gamma ray maps produced by the Lunar Prospector GRS (i.e., Feldman et al., 1999; Prettyman et al., 2002). The South Pole Aitken basin, which is a type of mare feature, is also visible in the map. The brightest and dimmest pixels differ by ~0.8%, which is 10 times the statistical uncertainty of ~0.0008.

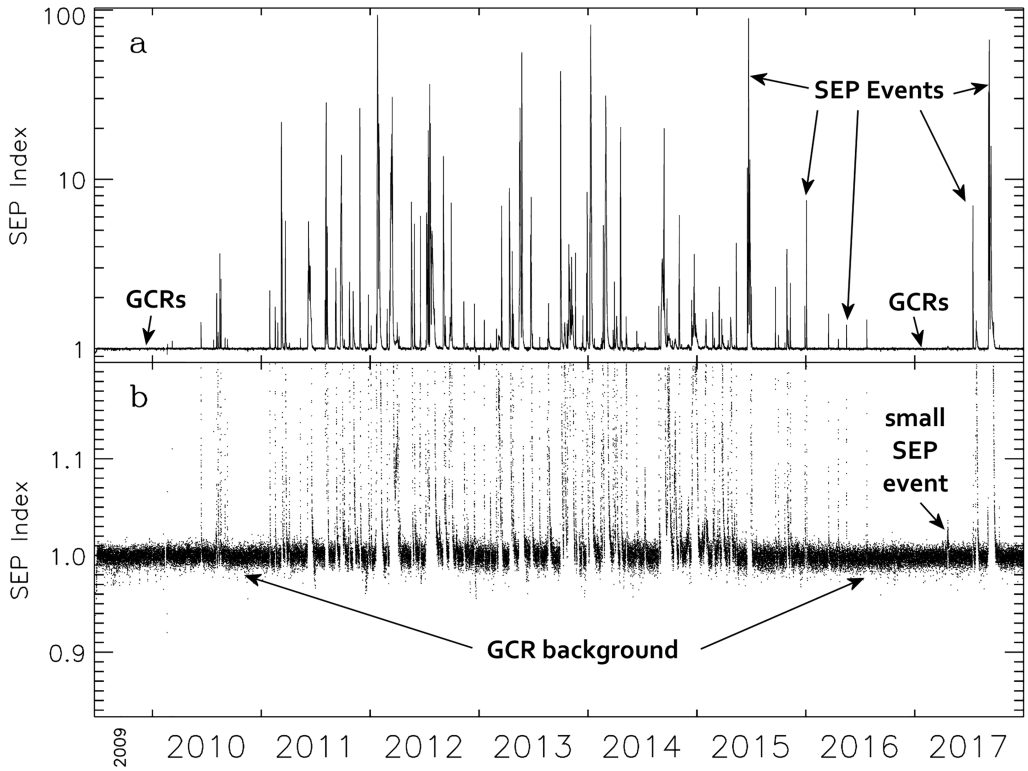

Figure 2. Time history of the SEP Index in 1-hr intervals. (a) Plot showing the full range of SEP Index values. (b) Same plot magnified to show details in the GCR-caused background, which is remarkably flat on all time scales. Very small SEP events stand out clearly from the background. The SEP Index value due to the GCR background varies from its average by only ~1% during solar quiet times.

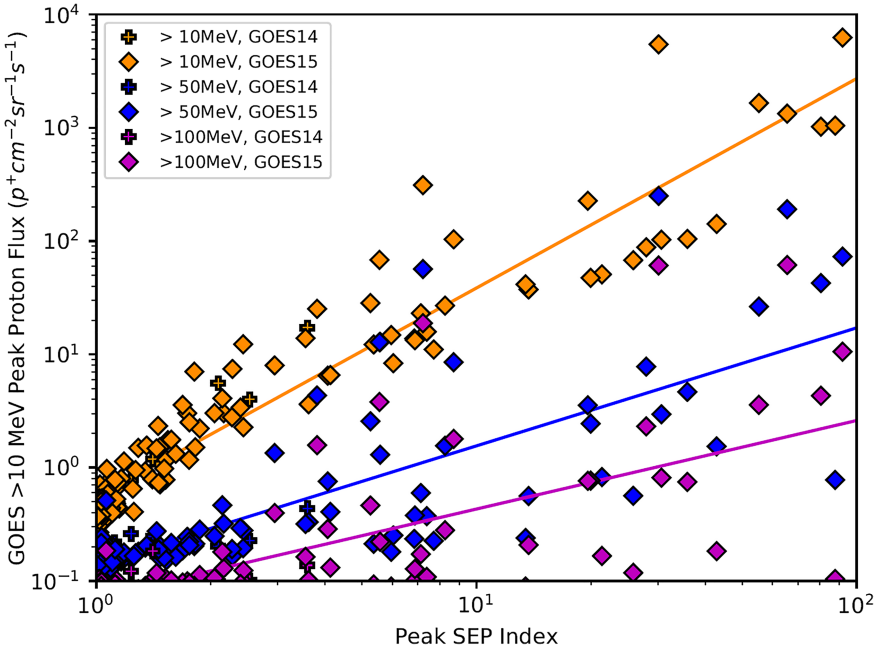

Figure 3. Comparison of SEP event magnitudes as determined by the maximum SEP Index values during each event (*x* axis) and the GOES 14 or 15 peak proton flux >10 MeV (yellow), >50 MeV (blue), and >100 MeV (purple) during each event (*y* axis; data from Gurman, 2017). We fit the distribution of points from each energy channel with a power law (solid lines) to determine the relative correlation of the GOES and SEPI measurements; the correlation coeffiecients are 0.96 for >10 MeV, 0.80 for >50 MeV, and 0.71 for >100 MeV.

The variations in the map are most likely caused by particles affecting detector D6, which is the least-shielded Moon-facing detector in CRaTER. D6 should be the most sensitive to a wide range of albedo particles from the Moon, including protons, neutrons, and gamma rays. Since D6 appears in the numerator of one of the terms in the SEPI function, variations in SEPI with lunar location suggest that albedo particles from the Moon are primarily affecting the D6 detection rate, where they appear in SEPI as higher values for higher fluxes. Thus, spatial variations in SEPI probably correspond to fixed geological/elemental features on the Moon that affect the albedo yields of such particles.

6. Correlations With Other Moon Elemental/Spallation Maps

We use the Spearman rank correlation to compare the SEPI map with other lunar maps of spallation products and list the results in Table 1. The highest positive rank correlations with the SEPI map are the Lunar Prospector maps of gamma rays characteristic of thorium and iron nuclei, with values of ~0.74 in 15° binning, and ~0.76 in 20° binning. Gamma rays characteristic of aluminum nuclei measured by LP and thermal neutrons measured by LRO/LEND are the most anticorrelated to the SEPI map, with a correlation magnitude nearly identical to that for gamma rays characteristic of thorium and iron nuclei. These correlations suggest that SEPI is mapping an albedo particle enhancement from heavy elements that are concentrated in the maria. We next address to which types of albedo particles the SEPI map might correspond.

7. Candidate Albedo Particles in the SEPI Map

While all previous lunar mapping with CRaTER data used analysis that focused on albedo protons (Schwadron et al., 2016, 2018; Wilson et al., 2012, 2014), we use here singles rates to derive the SEP Index and map the Moon. This means that we are probably seeing map features from more than one type of albedo particle. Albedo protons, neutrons, and gamma ray photons are all expected to contribute to the singles rate in D6, so we address each of these here.

7.1. Albedo Protons

Previous studies used two-detector coincident energy signatures to isolate lunar albedo protons in CRaTER data, so we know that albedo protons account for some fraction of D6 detections and therefore may be partly responsible for the features in the SEPI map. Wilson et al. (2012) and Schwadron et al. (2016, 2018) considered albedo protons that passed through both D4 and D6, which requires an incident proton kinetic energy of at least 64 MeV. Such albedo protons cause little increase of the D6 rate relative to the D1, D3 and D4 rates, as these protons have enough energy to reach both D6 and D4 when arriving from the nadir direction and can reach every CRaTER detector when impinging on the side of CRaTER. In other words, the SEP Index is relatively insensitive to these types of protons.

In contrast to the coincident data studies of Wilson et al. (2012) and Schwadron et al. (2016, 2018), the SEPI map should reveal only albedo protons with energies between ~14 and ~50 MeV; the former is the minimum energy required to pass through the nadir end cap of CRaTER and reach D6, while the latter is the maximum energy at which each of the six detectors is shielded from protons impinging from the side (Spence et al., 2010). Side-penetrating protons above 50 MeV can reach all six detectors, and thus contribute to D1, D3, and D4, which offsets their signal in D6 and leaves SEPI relatively unchanged. On the other hand, protons below 50 MeV that approach CRaTER detectors D1–D4 from either the side or from nadir are blocked by either external shielding or TEP, respectively, and do not contribute to the D1, D3, and D4 detection rates (see Figure 2). Thus, the SEPI mapping method may complement the earlier mapping methods (protons >64 MeV) by selecting a different part of the albedo proton energy spectrum (14–50 MeV). If so, we may be able to diagnose the specific nuclear spallation processes responsible for producing the albedo protons.

7.2. Neutrons

Some fraction of the particles represented in SEPI may be secondary particles produced within the CRaTER instrument by lunar albedo neutrons colliding with atoms in CRaTER. Geant4 simulations found that albedo neutrons contribute ~1% of the particle count rate in D6, comparable to the contrast in the SEPI map; they also found triple-coincidence neutrons (albedo neutrons that traverse the entire length of CRaTER and trigger all three thick detectors) are negligible compared to other particles (Looper et al., 2013). The high inverse correlation between the SEPI map and thermal neutron maps suggests that any

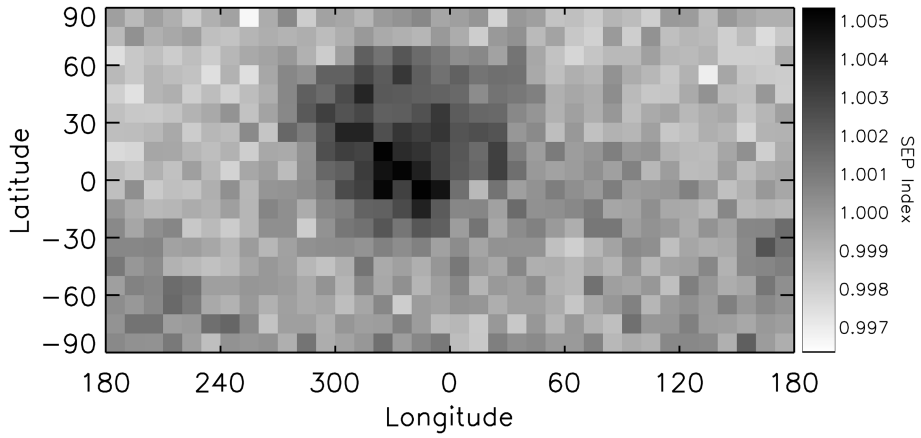

Figure 4. Cylindrical lunar map of SEPI with 10° × 10° binning. The lunar maria on the Earth-facing hemisphere generally have up to a 0.5% higher SEPI value than the highlands, and the South Pole Aitken Basin (bottom left and bottom right) is also slightly higher. Each pixel's value has an uncertainty of ~0.0008, or ~10% of the map's full dynamic range.

thermal neutron signal in SEPI is being overpowered by a stronger signal with a positive correlation to SEPI, such as protons or gamma rays. We will further explore the connection between SEPI and thermal neutrons in future work.

7.3. Gamma Rays

Like neutrons, gamma ray photons from the Moon can pass into the CRaTER instrument and interact with matter to produce particles that register in all of CRaTER's detectors, as predicted in simulations (Looper et al., 2013) and demonstrated in laboratory calibrations of the CRaTER instrument (Spence et al., 2010).

Table 1
Spearman Rank Correlation With SEPI Map

	15° × 15° binning		20° × 20° binning	
Map[†]	Rank correlation coefficient	Significance of deviation from zero*	Rank correlation coefficient	Significance of deviation from zero*
Thorium (γ)[a,f]	**0.744**	<0.001	**0.780**	<0.001
Iron (γ)[a,f]	**0.732**	<0.001	**0.753**	<0.001
Titanium (γ)[a,f]	0.641	<0.001	0.657	<0.001
LP fast neutrons[b,f]	0.627	<0.001	0.665	<0.001
Potassium (γ)[a,f]	0.532	<0.001	0.535	<0.001
LEND CSETN[e]	0.476	<0.001	0.492	<0.001
LEND SETN[e]	−0.127	0.031	−0.122	0.121
Silicon (γ)[a,f]	−0.274	<0.001	−0.260	<0.001
LP epithermal neutrons[c,f]	−0.420	<0.001	−0.433	<0.001
Calcium (γ)[a,f]	−0.656	<0.001	−0.678	<0.001
Aluminum (γ)[a,f]	**−0.711**	<0.001	**−0.761**	<0.001
LP thermal neutrons[d,f]	**−0.712**	<0.001	**−0.741**	<0.001
LEND ST3[e]	**−0.741**	<0.001	**−0.768**	<0.001

*Range is from 1 (not significant) to 0 (very significant). [†]Maps with largest correlation or anti-correlation to SEPI map in bold. [a]Feldman et al. (1999) and Prettyman et al. (2002). [b]Maurice et al. (2000, 2004). [c]Feldman, Lawrence, Elphic, Barraclough, et al., 2000, Feldman et al., 2001) and Maurice et al. (2004). [d]Feldman, Lawrence, Elphic, Vaniman, et al. (2000), Elphic et al. (2000), and Maurice et al. (2004). [e]Litvak, Mitrofanov, Sanin, Golovin, et al., 2012, Litvak, Mitrofanov, Sanin, Malakhov, et al., 2012). [f]Feldman et al. (2019).

The detector that is least shielded from the nadir direction, D6, should record more counts from albedo gamma rays than the other more shielded detectors. It is beyond the scope of this paper to quantify the detection efficiencies of gamma rays in CRaTER, as gamma ray interaction with matter is a complex topic. We simply note that the SEPI map most closely resembles maps of lunar gamma rays characteristic of iron and thorium nuclei and leave in-depth analysis of the gamma ray contribution to SEPI for future work. Of interest will be identifying gamma ray features in energy-deposit spectra from CRaTER's primary data product to possibly identify specific elements in the surface regolith that contribute to SEPI features.

8. Conclusions

The SEP Index, which is a function of the total detection rates from four of CRaTER's six detectors, is a simple empirical method for discerning SEP events in the CRaTER data archive. We derived the index using the principle that CRaTER's midstack detectors (D3 and D4) are more shielded from SEPs than the end detectors (D1 and D6), and the final weighting of the terms in the SEP Index was derived empirically to minimize the variation of the index value during solar quiet times. The index is sufficiently steady during quiet periods to make even very small SEP events stand out clearly in plot of the SEP Index versus time. Future designs for radiation monitors in crewed missions may be able to take advantage of this principle to provide the earliest possible warnings of the onset of SEP events from local instrument data.

The lunar SEPI map has produced CRaTER's clearest map yet of lunar albedo particle variations and reflects an as-yet unknown combination of lunar albedo protons, neutrons, and gamma rays. The map is derived from the SEP Index during solar quiet periods, and probably represents an excess albedo particle signal in the Moon-facing D6 detector. The SEPI map suggests that CRaTER may be able to complement gamma ray and/or neutron data from other instruments and missions, and it may also be measuring a second, lower energy albedo proton population (14–50 MeV) that complements previous mapping studies of higher-energy albedo protons (>64 MeV) that sample the top ~10 cm of lunar regolith. The map most closely resembles Lunar Prospector maps of gamma rays characteristic of thorium and iron nuclei, while being closely anticorrelated with gamma rays characteristic of aluminum nuclei and thermal neutrons measured by Lunar Prospector and LRO/LEND. We will build on this result with a range of follow-up studies, including the refinement of the latitudinal and diurnal trends in regolith hydrogenation with the SEPI mapping method, quantification of CRaTER's sensitivity to neutrons, and a search for gamma ray spectral features in CRaTER energy-deposit spectra.

Acknowledgments
The science data used in this paper are available at the NASA PDS PPI node as "3/4-DDR-PROCESSED" files (Knopf & Sharlow, 2009), and both the science data and spacecraft geometry data are available at the CRaTER Data Archive at the University of New Hampshire (Schwadron et al., 2019) as "Level 2 Data" files and "Ephemeris/Pointing" files, respectively. The GOES data are available at https://satdat.ngdc.noaa.gov/sem/goes/data/avg/. This work was funded by the NASA LRO mission and the NASA DREAM^2 program.

References

Case, A. W., Kasper, J. C., Spence, H. E., Zeitlin, C. J., Looper, M. D., Golightly, M. J., et al. (2013). The deep space galactic cosmic ray lineal energy spectrum at solar minimum. *Space Weather*, *11*, 361–368. https://doi.org/10.1002/swe.20051

Desai, M., & Giacalone, J. (2016). Large gradual solar energetic particle events. *Living Reviews in Solar Physics*, *13*(1), 3. https://doi.org/10.1007/s41116-016-0002-5

Elphic, R. C., Lawrence, D. J., Feldman, W. C., Barraclough, B. L., Maurice, S., Binder, A. B., & Lucey, P. G. (2000). Lunar rare earth element distribution and ramifications for FeO and TiO_2: Lunar Prospector neutron spectrometer observations. *Journal of Geophysical Research*, *105*(E8), 20,333–20,345. https://doi.org/10.1029/1999JE001176

Feldman, W. C., Barraclough, B. L., Fuller, K. R., Lawrence, D. J., Maurice, S., Miller, M. C., et al. (1999). The Lunar Prospector gamma-ray and neutron spectrometers, nuclear instruments and methods in. *Physics Research A*, *422*, 562–566. https://doi.org/10.1016/S0168-9002(98)00934-6

Feldman, W. C., Lawrence, D. J., Elphic, R. C., Barraclough, B. L., Maurice, S., Genetay, I., & Binder, A. B. (2000). Polar hydrogen deposits on the Moon. *Journal of Geophysical Research*, *105*, 4175–4195. https://doi.org/10.1029/1999JE001129

Feldman, W. C., Lawrence, D. J., Elphic, R. C., Vaniman, D. T., Thomsen, D. R., Barraclough, B. L., et al. (2000). The chemical information content of lunar thermal and epithermal neutrons. *Journal of Geophysical Research*, *105*, 20,347–20,363. https://doi.org/10.1029/1999JE001183

Feldman, W. C., Maurice, S., Lawrence, D. J., Little, R. C., Lawson, S. L., Gasnault, O., et al. (2001). Evidence for water ice near lunar poles. *Journal of Geophysical Research*, *106*, 23,231–23,251. https://doi.org/10.1029/2000JE001444

Feldman, W. C., Prettyman, T. H., Belian, R. D., Elphic, R. C., Gasnault, O., Lawrence, D. J., et al. (2019). Lunar Prospector reduced spetrometer data: Special products. [online] Available at: https://pds-geosciences.wustl.edu/missions/lunarp/reduced_special.html

Gurman, J. B. (2017). Solar proton events, 1976–present. [online] Available at: https://umbra.nascom.nasa.gov/SEP/

Joyce, C. J., Schwadron, N. A., Wilson, J. K., Spence, H. E., Kasper, J. C., Golightly, M., et al. (2013). Validation of PREDICCS using LRO/CRaTER observations during three major solar events in 2012. *Space Weather*, *11*, 350–360. https://doi.org/10.1002/swe.20059

Knopf, W., & Sharlow, M. (2009). PDS/PPI Home Page; Lunar Reconnaissance Orbiter (LRO). [online] Available at: https://pds-ppi.igpp.ucla.edu/search/?t=Earth (Moon)&sc=Lunar_Reconnaissance_Orbiter_(LRO)

Lawrence, D. J., Feldman, W. C., Barraclough, B. L., Binder, A. B., Elphic, R. C., Maurice, S., & Thomsen, D. R. (1998). Global elemental maps of the Moon: The Lunar Prospector gamma-ray spectrometer. *Science*, *281*(5382), 1484–1489. https://doi.org/10.1126/science.281.5382.1484

Litvak, M. L., Mitrofanov, I. G., Sanin, A., Malakhov, A., Boynton, W. V., Chin, G., et al. (2012). Global maps of lunar neutron fluxes from the LEND instrument. *Journal of Geophysical Research*, *117*, E00H22. https://doi.org/10.1029/2011JE003949

Litvak, M. L., Mitrofanov, I. G., Sanin, A. B., Golovin, D. V., Malakhov, A. V., Boynton, W. V., et al. (2012). LEND neutron data processing for the mapping of the Moon. *Journal of Geophysical Research*, *117*, E00H32. https://doi.org/10.1029/2011JE004035

Looper, M. D., Mazur, J. E., Blake, J. B., Spence, H. E., Schwadron, N. A., Golightly, M. J., et al. (2013). The radiation environment near the lunar surface: CRaTER observations and Geant4 simulations. *Space Weather*, *11*, 142–152. https://doi.org/10.1002/swe.20034

Maurice, S., Feldman, W. C., Lawrence, D. J., Gasnault, O., d'Uston, C., & Lucey, P. G. (2000). High-energy neutrons from the Moon. *Journal of Geophysical Research*, *105*, 20,365–20,375. https://doi.org/10.1029/1999JE001151

Maurice, S., Lawrence, D. J., Feldman, W. C., Elphic, R. C., & Gasnault, O. (2004). Reduction of neutron data from Lunar Prospector. *Journal of Geophysical Research*, *109*, E07S04. https://doi.org/10.1029/2003JE002208

Mitrofanov, I. G., Sanin, A. B., Boynton, W. V., Chin, G., Garvin, J. B., Golovin, D., et al. (2010). Hydrogen mapping of the lunar south pole using the LRO neutron detector experiment LEND. *Science*, *330*(6003), 483–486. https://doi.org/10.1126/science.1185696

Potgieter, M. S. (2013). Solar modulation of cosmic rays. *Living Reviews in Solar Physics*, *10*(1), 3.

Prettyman, T. H., Feldman, W. C., Lawrence, D. J., McKinney, G. W., Binder, A. B., Elphic, R. C., et al. (2002). Library least squares analysis of Lunar Prospector gamma-ray spectra, 33rd Lunar and Planetary Science Conference, Abstract #2012.

Prettyman, T. H., Hagerty, J. J., Elphic, R. C., Feldman, W. C., Lawrence, D. J., McKinney, G. W., & Vaniman, D. T. (2006). Elemental composition of the lunar surface: Analysis of gamma ray spectroscopy data from Lunar Prospector. *Journal of Geophysical Research*, *111*, E12007. https://doi.org/10.1029/2005JE002656

Schwadron, N. A., Spence, H. E., & Wilson, J. K. (2019). CRaTER data products. [online] Available at: http://crater-web.sr.unh.edu/

Schwadron, N. A., Blake, J. B., Case, A. W., Joyce, C. J., Kasper, J., Mazur, J., et al. (2014). Does the worsening galactic cosmic radiation environment observed by CRaTER preclude future manned deep space exploration? *Space Weather*, *12*, 622–632. https://doi.org/10.1002/2014SW001084

Schwadron, N. A., Wilson, J. K., Jordan, A. P., Looper, M. D., Zeitlin, C., Townsend, L. W., et al. (2018). Using proton radiation from the Moon to search for diurnal variation of regolith hydrogenation. *Planetary and Space Science*, *162*, 113–132. https://doi.org/10.1016/j.pss.2017.09.012

Schwadron, N. A., Wilson, J. K., Looper, M. D., Jordan, A. P., Spence, H. E., Blake, J. B., et al. (2016). Signatures of volatiles in the lunar proton albedo. *Icarus*, *273*, 25–35. https://doi.org/10.1016/j.icarus.2015.12.003

Spence, H. E., Case, A. W., Golightly, M. J., Heine, T., Larsen, B. A., Blake, J. B., et al. (2010). CRaTER: The cosmic ray telescope for the effects of radiation experiment on the lunar reconnaissance orbiter mission. *Space Science Reviews*, *150*(1-4), 243–284. https://doi.org/10.1007/s11214-009-9584-8

Spence, H. E., Golightly, M. J., Joyce, C. J., Looper, M. D., Schwadron, N. A., Smith, S. S., et al. (2013). Relative contributions of galactic cosmic rays and lunar proton "albedo" to dose and dose rates near the Moon. *Space Weather*, *11*, 643–650. https://doi.org/10.1002/2013SW000995

Wilson, J. K., Schwadron, N., Spence, H. E., Case, A. W., Golightly, M. J., Jordan, A., et al. (2014). Lunar proton albedo anomalies: Soil, surveyors, and statistics, abstract P13D-3853, American Geophysical Union Fall Meeting.

Wilson, J. K., Spence, H. E., Kasper, J., Golightly, M., Bern Blake, J., Mazur, J. E., et al. (2012). The first cosmic ray albedo proton map of the Moon. *Journal of Geophysical Research*, *117*, E00H23. https://doi.org/10.1029/2011JE003921

Zeitlin, C., Case, A. W., Spence, H. E., Schwadron, N. A., Golightly, M., Wilson, J. K., et al. (2013). Measurements of galactic cosmic ray shielding with the CRaTER instrument. *Space Weather*, *11*, 284–296. https://doi.org/10.1002/swe.20043